NANO LETTERS

Letter

pubs.acs.org/NanoLett

Rethinking Coal: Thin Films of Solution Processed Natural Carbon Nanoparticles for Electronic Devices

Brent D. Keller, Nicola Ferralis,* and Jeffrey C. Grossman*

Department of Materials Science and Engineering, Massachusetts Institute of Technology, 77 Massachusetts Avenue, Cambridge, Massachusetts 02139, United States

Supporting Information

ABSTRACT: Disordered carbon materials, both amorphous and with long-range order, have been used in a variety of applications, from conductive additives and contact materials to transistors and photovoltaics. Here we show a flexible solution-based method of preparing thin films with tunable electrical properties from suspensions of ball-milled coals following centrifugation. The as-prepared films retain the rich carbon chemistry of the starting coals with conductivities ranging over orders of magnitude, and thermal treatment of the resulting films further tunes the electrical conductivity in excess of 7 orders of magnitude. Optical absorption measurements demonstrate tunable optical gaps from 0 to 1.8 eV. Through low-temperature conductivity measurements and Raman spectroscopy, we demonstrate that variable range hopping controls the electrical properties in as-prepared and thermally treated films and that annealing increases the sp^2 content, localization length, and disorder. The measured hopping energies demonstrate electronic properties similar to amorphous carbon materials and reduced graphene oxide. Finally, Joule heating devices were fabricated from coal-based films, and temperatures as high as 285 °C with excellent stability were achieved.

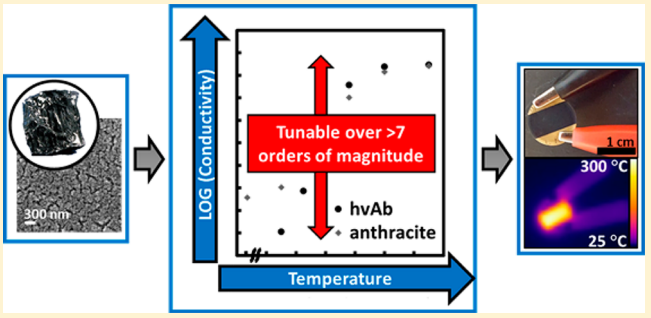

KEYWORDS: *Coal, amorphous carbon, organic semiconductors, thin films, solution processing*

Carbon has long been known as one of the most chemically versatile elements. As a result, carbonaceous materials have been of technological interest for their wide range of electronic properties—resulting in materials ranging from low cost conducting materials such as graphite and carbon black, to semiconducting fullerenes and carbon nanotubes, and to insulating diamond and diamond-like carbon. Specifically, carbon black, carbon filaments, and other carbon materials are used in electrodes, conductivity additives, and electromagnetic reflectors.[1] Graphitic materials[2] and amorphous carbon (a-C)[3,4] are the leading and a promising candidate, respectively, for anode materials in lithium ion batteries. Amorphous carbon has also been used in the manufacturing of transistors[5,6] and photovoltaic devices,[7,8] and nanostructured graphitic materials (such as graphene and reduced graphene oxide) have gained significant attention for applications including in photovoltaics,[9−11] transparent conductive membranes,[12−16] and Joule heating devices.[17−19]

Despite decades of research on synthetically processed carbon materials, facile, tunable,[20] low-temperature, solution processing methods remain elusive. Carbon black synthesis requires temperatures as high as 2000 °C,[21] and a-C is typically deposited by plasma-enhanced chemical vapor deposition (CVD)[22,23] although aerosol-assisted CVD has recently been demonstrated.[8] While extensive research has been conducted to develop solution-based methods of graphene deposition, rGO films remain several orders of magnitude less conductive than CVD graphene.[16,24,25]

In contrast to the widely studied world of synthetic carbonaceous materials, the optical and electronic properties (and corresponding range of tunability) of natural carbonaceous materials are still poorly understood. Yet, this gap in understanding is worth bridging, particularly given the massive global availability of low cost naturally formed carbonaceous materials (for example, nearly 8 gigatonnes per year of coal is produced globally at ∼0.05 $/kg).[26] Such materials may find uses beyond combustion in many of the applications in which synthetic carbon materials are currently being deployed. Because of the wide array of molecular compounds present in different natural carbonaceous materials (from aromatic to aliphatic, with a varying degree of functional chemistry),[27] these materials could provide a broad range of electrical properties at extremely low cost. In order to unlock the potential of these materials, it is crucial to develop compatible, low cost methods of processing them, characterize the nanostructure of such processed films, and measure their optical and electrical properties including a detailed understating of the dominant charge transport mechanisms. To date, electrical conductivity

Received: November 19, 2015
Revised: March 12, 2016

DOI: 10.1021/acs.nanolett.5b04735
Nano Lett. XXXX, XXX, XXX−XXX

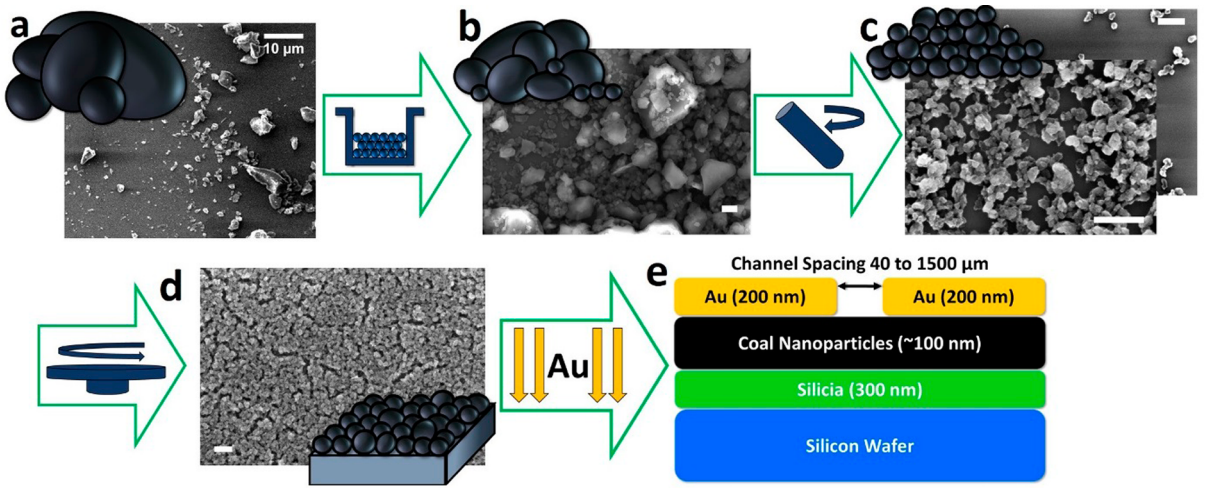

Figure 1. Preparation of organic thin films from naturally sourced carbon. As-received powders (a) were first milled in a stainless steel ball mill to produce a broad distribution of particle size. (b) Sub-100 nm size particles were then selected by centrifugation, (c), and spin coating was used to produce thin films, (d). (e) Thermal evaporation of gold was used to deposit electrical contacts with shadow masking used to define channels ranging from 40 to 1500 μm. All scale bars are 300 nm unless otherwise specified.

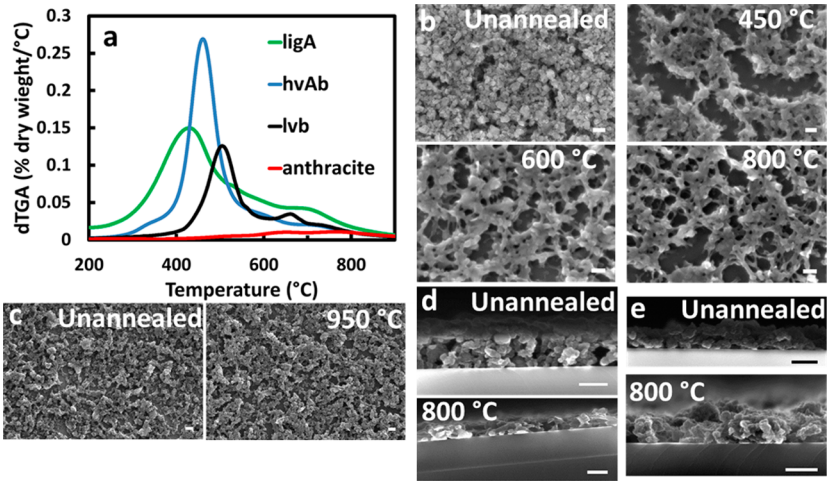

Figure 2. Morphological effects of thermal processing of coal thin films. (a) Differential TGA showing the temperatures at which decomposition peaks occur in each coal. All coals show a low rate of decomposition rate by 900 °C with less mature coals[30] showing primary mass loss at lower temperatures. Representative SEM images of hvAb (b) and anthracite (c) nanoparticle films after annealing at several temperatures showing both extensive mass loss and sintering of the hvAb particles between room temperature and 600 °C. Because of much lower mass loss, the anthracite films show little morphological change. Cross-sectional SEM of hvAb (d) and anthracite (e) showing the thickness of films before and after 800 °C annealing. All scale bars are 200 nm.

has been measured in coals and coal char, but solely for the purpose of correlating in situ conductivity measurements to fuel processing as part of underground coal gasification programs.[28,29]

In this work, we present a method for solution processing sub-100 nm natural carbon particles from standard coal sources to obtain 100 nm thick coal films and characterize their microstructure by scanning electron microscopy (SEM). We relate the carbon bonding configuration (characterized with Raman spectroscopy) to the conductivity, optical absorption properties, and the dominant charge transport mechanism, through variable temperature (50 K to room temperature) current−voltage measurements. Finally, annealing of these films up to temperatures as high as 950 °C was explored as a method for further tailoring the properties of natural carbon films beyond the precursor chemical phase space. We show this simple annealing process leads to a direct modification of the sp^2 content and aromatic domain size, which allows for the film electrical conductivity to vary over 7 orders of magnitude.

Figure 1 illustrates the approach taken to produce thin films of natural carbon. As received coal powders were ball milled for up to 106 h. Over this extended milling period, particle size continued to decrease (Supporting Information Figure S1). Dilutions of the resulting material were centrifuged to select smaller particles less than 100 nm in diameter from the dispersion (Figure 1c), and spin coating was used to then prepare thin films for device fabrication from the supernatant (Figure 1d). The milling and centrifugation process did not cause changes in the carbon hybridization chemistry or bonding structure as determined by both X-ray photoelectron spectroscopy (XPS) and Raman spectroscopy (Supporting Information Figures S2 and S3). Thus, this method can be applied to natural carbon materials to produce thin films without narrowing the resulting thin film chemistries. Ball milling offers a solution

DOI: 10.1021/acs.nanolett.5b04735
Nano Lett. XXXX, XXX, XXX−XXX

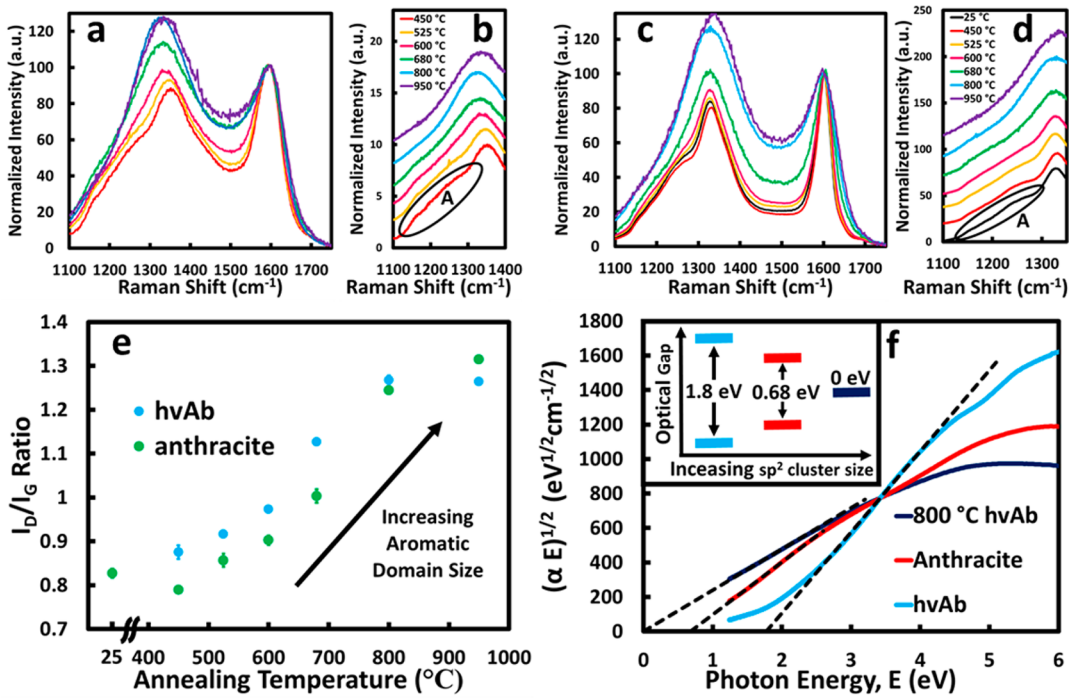

Figure 3. Tunability of chemical structure in coal films. Raman spectra (normalized by the G peak maximum) of hvAb (a,b) and anthracite (c,d) nanoparticle films after different annealing conditions. Annealing shows a clear increase in the I_D/I_G ratio and broadening of the G peak, indicative of increasing disorder in sp^2 domains. D shoulder band regions of hvAb (b) and anthracite (d), corresponding to reduced hydrogen content, specifically the loss of the shoulder peak, A (circled for lowest temperature). (e) Plot of the ratio D peak maximum to G complex maximum suggesting a steady increase in the relative aromatic content of the films in the 0.5 to 2 nm aromatic domain size regime. Error bars represent standard errors based on at least three measurements in different regions of the film. (f) Plot of the square root of the product of α and E as a function of photon energy as determined by optical absorption spectroscopy. The x-intercepts of the fits of the linear regions (dashed lines) give the values of the optical bad gap. The inset shows a schematic of the optical gaps calculated for hvAb, anthracite, and 800 °C annealed hvAb films arranged by increasing sp^2 cluster size.

processing approach for the application of the entire coal phase space studied to thin film devices. Material was processed both in air and under nitrogen with no differences observed. Particle suspensions were stored in isopropanol under air for as long as a year with no chemical changes as measured by Raman and XPS.

In order to use natural carbonaceous materials in electrical applications, the morphology of the thin films must be understood as it plays a critical role in carrier mobility and extraction, as well as separation and surface recombination in many applications. While milling was shown to preserve the starting carbon hybridization chemistry and bonding structure for each coal, different coals showed widely varying morphologies after ball milling and after spin coating. The four coals studied in order of increasing rank, or degree of maturation, were Department of Energy Coal Sample (DECS) 25 (lignite A), DECS 31 (high volatile A bituminous - hvAb), DECS 19 (low volatile bituminous), and DECS 21 (anthracite).[30] The particle size distribution after milling varied across the coals studied (Supporting Information Figure S4). In particular, a significant portion of large (5−10 μm) particles remains in the anthracite suspension, although all suspensions include numerous sub-100 nm particles. Following centrifugation, these smaller particles can be selected from the suspensions with the colloidal stability also varying across the coals (Supporting Information Figure S5). While sub-100 nm dispersions could be achieved with any of the coals through appropriate choice of centrifugation speed and duration, the hvAb produced the thin films with the most uniform thickness and only moderate cracking of the film (Figure 1d) when isopropanol was used as a solvent.

Tunability across a broad phase space is critical for tailoring a material to a specific application. To develop a direct method of modifying the properties of a film beyond the choice of a starting coal, annealing at elevated temperature under argon gas was also performed. The less mature the coal (i.e., the higher the aliphatic content), the earlier the onset of thermal decomposition (thermogravimetric analysis, (TGA) Figure 2a), as has been observed elsewhere.[31] Temperatures as low as 300 °C were observed to impact the properties of hvAb and even quite mature coals experience chemical changes at sufficiently high temperatures. Scanning electron micrographs of hvAb and anthracite films at several annealing temperatures (Figures 2b,c), show that annealing causes sintering of the particles and amplification of cracks in the films. However, the morphology remains consistent above 450 °C. Because of the smaller mass loss in the higher rank anthracite, the morphological changes from annealing are less pronounced than in hvAb. It is important to note that the temperatures used remain much lower than those used for production of materials such as carbon black. Furthermore, the tunable electronic properties achieved through annealing can also be realized using a lower temperature annealed or unannealed precursor coal of different rank, as will be shown below.

Beyond understanding the nanoscale morphology, natural carbon materials must also be characterized at the level of chemical functionalities, and the impact on the optical properties, electrical conductivity, and carrier transport under-

DOI: 10.1021/acs.nanolett.5b04735
Nano Lett. XXXX, XXX, XXX−XXX

stood. The characterization of the type of carbon chemistries present in any given film is critical to identifying the appropriate coal material for applications ranging from battery anodes, where specific binding is needed, to transistors and photovoltaics, where electronic state traps associated with specific chemical structures can control device performance. Raman spectra (Figure 3) of hvAb and anthracite films at several annealing temperatures provide insight into the changes in the carbon bonding structure. Above 450 °C, the ratio of peak heights of the D and G Raman bands (I_D/I_G) steadily increases indicating increasing sp^2 cluster size in the 0.5 to 2 nm regime (Figure 3e) as shown previously in a-C,[32,33] graphite,[34] and graphene.[35,36] There is also a progressive decrease in the intensity of the D shoulder band from 1150 to 1300 cm^{-1} (Figure 3b,d) that corresponds to decreasing aliphatics.[37] Anthracite, which has a higher sp^2 content before annealing, shows minimal change in the sp^2 bonding network as determined by Raman spectroscopy up to 450 °C (Figure 3c). However, annealing at 950 °C causes similar changes to those observed in hvAb as well as broadening of the G-peak indicating an increase in the variety and disorder of sp^2 domains[32] that was more modest in hvAb due to a larger initial G peak width. In contrast to the physical morphology of the films (Figure 2) in which anthracite is observed to undergo a much smaller transformation than hvAb, both coals show similar changes in the carbon bonding configuration for the highest annealing temperatures. Thus, we conclude that annealing up to approximately 600 °C results in a large reduction in aliphatics and a modest increase in sp^2 localization length and disorder. However, annealing between approximately 600 and 950 °C causes a dramatic increase in carbon bond disorder and a rapid conversion to an aromatic rich a-C structure with increasing domain size at higher temperature.

The optical energy bandgap is a critical property for design of light absorbing or emitting devices, such as photovoltaics or photosensors. To demonstrate the variation of the optical bandgaps across the natural carbon phase space and its modification with thermal processing, optical absorption spectroscopy was performed. Using the method developed by Tauc et al.[38] to determine the value of an optical bandgap, a function of the product of the absorbance (α) and the photon energy (E) may be plotted as a function of photon energy and the x-intercept of a fit of the linear region gives the value of the optical band gap (Figure 3f). Because slightly different treatments of the density of states and matrix elements gives rise to different functional forms to be plotted on the ordinate,[39] we have used the square root of the product of the absorbance and the photon energy, $(\alpha E)^{1/2}$, as it is appropriate for the electrical states of a-C and hydrogenated amorphous carbon (a-C:H)[22] and fits the data reported here well. This optical gap is associated with π to π^* band transitions in the aromatic domains, and we report values of 0.68 eV in anthracite and 1.8 eV in hvAb films. Furthermore, thermal annealing of hvAb at 800 °C reduced the optical gap to 0 eV. This underscores the chemical and optical tunability as the choice of coal varies the optical gap of the aromatic domains from 1.8 to 0.68 eV, and thermal processing allows for extension of the aromatic domain size until elimination of the optical gap. Approximating the aromatic domains as compact clusters of six-membered rings and using the data prepared by Robertson et al.,[40,41] the values of these optical gaps correspond to sp^2 domains 0.9 nm in diameter (10 rings) in the hvAb and 2.2 nm in diameter (70 rings) in the anthracite, which is in good agreement with the I_D/I_G Raman peak ratios discussed earlier (Details in Supporting Information).

To quantify the effect of the tunable chemical structure observed through Raman and absorption spectroscopies on electrical performance, gold contacts were evaporated onto hvAb and anthracite films including those annealed at several temperatures. The current voltage relationship was found to be linear for all devices (Supporting Figure S6a). The conductance also varied with contact spacing (L) indicating that contact resistance is not dominant. By plotting the conductance of the film (σ) per contact width (w) as a function of the inverse of the distance between the contacts ($\sigma/wt = \sigma_0/L$), the conductivity of the films can be determined under an assumption of uniform contact resistance (see Supporting Information Figure S6b). Uniform film thicknesses (t) of 100 nm were assumed (Figure 2c,d). However, conductivity through the films is significantly more circuitous than a direct path between the contacts (Figure 2b) and it is also potentially limited by very thin regions of the film. Thus, the actual material conductivity is most likely larger than the film conductivity values measured.

Without annealing, the hvAb films were not sufficiently conductive for the electrical conductivity to be measured. For hvAb films, measurable conductivity (>~10^{-6} S/m) was observed for films annealed above 450 °C, where it varied over 7 orders of magnitude before saturation. Figure 4a shows the conductivity of these films compared to several synthetic carbon materials under active research. The electrical conductivities observed are broadly tunable over a range of materials such as rGO and a-C by varying the annealing temperature. Films of unannealed anthracite possess conductivity comparable to that of a ~500 °C annealed hvAb film, emphasizing the degree of chemical and therefore property variability of the precursor coals without the need for high-temperature annealing. At an annealing temperature of 950 °C, the anthracite shows a transition to conductivity values similar to those of the highest temperature annealed hvAb, which is in good agreement with the similar sp^2 localization length (I_D/I_G ratio) observed in both films by Raman spectroscopy.

The optimization of device design relies on the knowledge of electronic transport mechanisms, that is, what limits the mobility and how carriers move through the material, allowing for a direct link between the bonding structure quantified by Raman and absorption spectroscopies and the wide tunability of electrical conductivity. To characterize this conduction mechanism, conductivity measurements were repeated at temperatures as low as 50 K. The observed trends follow the relationship predicted by variable range hopping in a three-dimensional material[42] or

$$\sigma \propto e^{-(T_0/T)^{1/4}} \tag{1}$$

where σ is the conductivity, T is the temperature, and $k_B T_0$ is the characteristic hopping energy or the average energy spacing near the Fermi level inside a volume defined by the wave function localization length, ξ, or

$$T_0 = \frac{1}{k_B \xi^3 N(E_F)} \tag{2}$$

where $N(E_F)$ is the density of states at the Fermi level. A plot of $\log_{10}(\sigma)$ as a function of $T^{-1/4}$ for the hvAb and anthracite films annealed at several temperatures is shown in Figure 4b,c, respectively. A linear behavior with a single T_0 value across the

DOI: 10.1021/acs.nanolett.5b04735
Nano Lett. XXXX, XXX, XXX−XXX

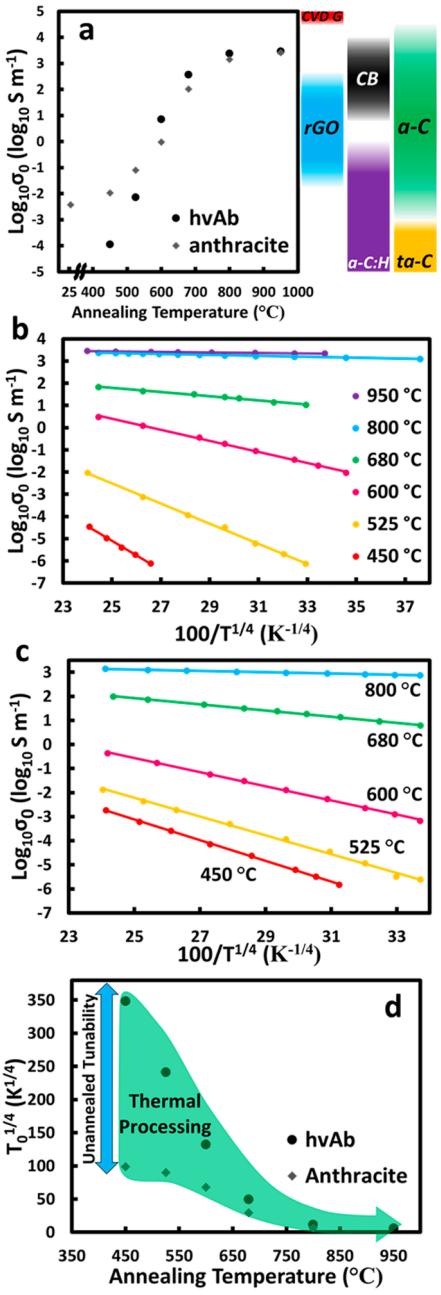

Figure 4. Conductivity and hopping transport in coal thin films. (a) Conductivity as determined from slope of σ/w as a function of $1/L$ for several annealing temperatures. By choice of annealing temperature, the conductivity can be tuned over 7 orders of magnitude. Typical range of conductivities reported from some synthetic carbon materials of research and commercial importance are included for reference, specifically, CVD grown graphene (CVD G),[14,16] rGO films,[12,13] carbon black (CB),[53,54] hydrogenated amorphous carbon (a-C:H),[55,56] a-C,[55,57,58] and tetrahedral amorphous carbon (ta-C).[6,23] Plot of the base 10 log of conductivity as a function of $T^{-1/4}$ for hvAb (b) and anthracite (c). Devices annealed at higher temperature show much weaker temperature dependence of conductivity due to an increase in the size and density of aromatic domains. Slope of best fit lines is related to $T_0^{1/4}$. (d) Plot of best-fit values of $T_0^{1/4}$ for films annealed at several temperatures. The large difference in $T_0^{1/4}$ values for hvAb and anthracite at low and medium annealing temperatures illustrates the diversity of structures and properties between coals. Annealing results in a conversion toward a minimal $T_0^{1/4}$ value indicating large and closely spaced aromatic domains.

temperature range for each sample is observed. For samples annealed at high temperatures, sp^2 domains are spaced closely both in energy and/or physical proximity, which gives rise to a small T_0. The values of $T_0^{1/4}$ are shown in Figure 4d as a function of the annealing temperature. The large difference in $T_0^{1/4}$ between the hvAb and anthracite for low and moderate annealing temperatures illustrates the variability in the electronic landscape accessible through the choice of natural carbon source. As the room-temperature conductivity approaches saturation after high-temperature annealing, the characteristic hopping energies of the two coals converge and approach a minimum. The values here reported are in good agreement with those for single flake rGO devices (20−140 $K^{1/3}$ depending strongly on the degree of reduction)[43,44] and a-C (from 220 $K^{1/4}$ for $\sigma = 10^{-5}$ S/m to 87 $K^{1/4}$ for $\sigma = 10^{0}$ S/m).[45,46] This demonstrates that in addition to possessing similar chemical properties, including the sp^2 domain size and amount of disorder, these properties result in the same conduction mechanism for the natural sourced carbon material and comparable synthetic materials such as a-C and rGO.

While an understanding of the work function and electrical mobility gap across the natural carbon phase space is needed for fabrication of band engineered devices such as transistors and photovoltaics, the ability to tune the conductivity in excess of 10^3 S/m opens up applications in Joule heating for medical,[47,48] defogging and defrosting,[18] lab-on-a-chip,[49] and other applications.[50] The low cost and abundance of natural carbon makes it attractive compared to complex materials such as doped tin oxides and singled-walled carbon nanotubes. Silver nanowire meshes, while solution processable, typically fail at temperatures ranging from 120 to 200 °C.[50,51] To demonstrate the performance of high-conductivity films made with naturally sourced carbon for stable high-temperature Joule heaters, anthracite films were deposited onto quartz substrates and annealed at 950 °C (Figure 5a). The temperature of the device

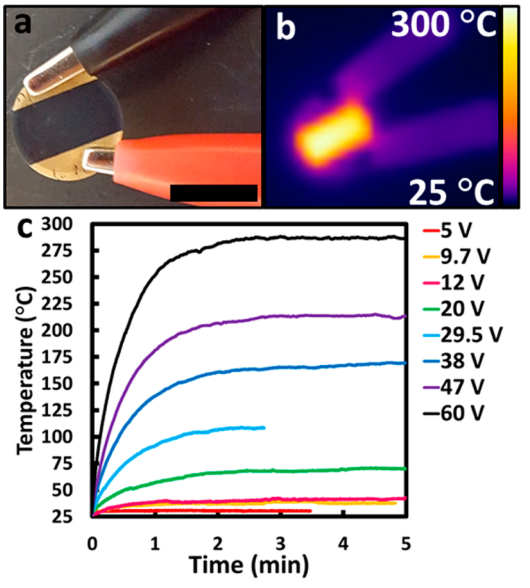

Figure 5. Joule heating devices fabricated from anthracite. (a) Optical image of anthracite film on quartz substrate during testing. Scale bar 1 cm. (b) Temperature map of device at 60 V bias showing heating to 285 °C with good uniformity away from contacts. (c) Maximum device temperature as a function of time for a representative device under several bias conditions showing heating response.

DOI: 10.1021/acs.nanolett.5b04735
Nano Lett. XXXX, XXX, XXX−XXX

was measured at biases up to 60 V and results in heating as high as 285 °C (Figure 5b,c), well beyond the region of instability of many silver films and comparable or exceeding 1000 °C annealed rGO and graphene-based devices under equal bias. The natural carbon films also had similar or better response times (less than 120 s) compared to rGO and graphene devices[18,19] and improved temperature uniformity across the device.[52] To further demonstrate the durability of the amorphous aromatic network, the films were maintained at 150 and greater than 200 °C for 30 min without deterioration in temperature (Figure S7).

In conclusion, we present a solution-based method of producing thin films of low-cost, widely available, natural carbon that preserves the broad chemical phase space of the starting material. Unlike several synthetic materials where the need for highly pure compositions adds to processing complexity and cost, the heterogeneous nature of natural carbon with its breadth of chemical functionalities, allows a single parameter, temperature, to carefully tune the optical and electrical properties of the material, in addition to C−H bond content, sp^2 domain size, and disorder. By use of low-temperature measurements, hopping transport was shown to govern the properties of the material in a manner comparable to rGO and a-C with a strong dependence on the size of sp^2 domains. Using the broad chemical phase space of coal and simple thermal annealing, the optical gap was shown to vary from 0 to 1.8 eV, and the conductivity was shown to be tunable over 7 orders of magnitude, a range that encapsulates many synthetic carbon materials of active research interest. Finally, the highest conductivity material was leveraged to fabricate Joule heating devices capable of reaching 285 °C without failure.

Recent years have witnessed a surge in scientific interest in the use of carbon materials such as a-C, graphene, and rGO as transparent conductive films, transistors, photovoltaics, and battery anodes. While promising research continues, limitations remain for these materials such as the reduced conductivity of rGO and need for plasma processing of a-C. Here, we have shown that solution processed thin films of low cost natural carbon such as coal possess a broad range of electrical properties that could be tapped for many of the same applications. Simple processing such as thermal annealing can further tune the chemical structure and electrical properties. Joule heating devices were demonstrated to achieve temperatures beyond many synthetic alternatives and performed as well or better than synthetic carbon devices. More fundamentally, this work shows the built-in chemical diversity of natural carbon provides opportunities in creative and innovative advanced materials applications, beyond its current use of primarily power generation through combustion.

■ ASSOCIATED CONTENT

Supporting Information

The Supporting Information is available free of charge on the ACS Publications website at DOI: 10.1021/acs.nanolett.5b04735.

Experimental methods, particle SEM and chemical characterization throughout processing, conductivity measurement, and details for sp^2 domain size calculation. (PDF)

■ AUTHOR INFORMATION

Corresponding Authors

*(J.C.G.) E-mail: jcg@mit.edu. Phone: (+1) 617-324-3566.
*(N.F.) E-mail: ferralis@mit.edu. Phone: (+1) 617-324-0372.

Author Contributions

The manuscript was written through contributions of all authors. All authors have given approval to the final version of the manuscript.

Notes

The authors declare no competing financial interest.

■ ACKNOWLEDGMENTS

We thank Matthew J. Smith for assistance in acquisition of some SEM images, Corentin Monmeyran for assistance in some of the low-temperature measurements of annealed hvAb films, Corinne R. Drysdale for assistance in measuring the conductivity of some of the anthracite devices at room temperature, and David Zhitomirsky for helpful discussions and assistance in Joule heating testing. We greatly appreciate seminal funding and support for this research from the Bose Fellows Program at MIT, which is a visionary program that provides researchers the opportunity to explore new, high-risk ideas. This work was partially supported by ExxonMobil under the MIT Energy Initiative (Grant EM09079), BK thanks the ExxonMobil Energy Fellow Program for partial support, and we appreciate helpful discussions with Mark Disko, Heather Elsen, Hans Thomann and Man Kit Ng. This work made use of the MRSEC Shared Experimental Facilities at MIT, supported by the National Science Foundation under award number DMR-1419807 and at the Center for Nanoscale Systems (CNS), a member of the National Nanotechnology Infrastructure Network (NNIN), which is supported by the National Science Foundation under NSF award no. ECS-0335765. CNS is part of Harvard University.

■ REFERENCES

(1) Chung, D. D. L. *J. Mater. Sci.* **2004**, *39*, 2645−2661.
(2) Persson, K.; Hinuma, Y.; Meng, Y.; Van der Ven, A.; Ceder, G. *Phys. Rev. B: Condens. Matter Mater. Phys.* **2010**, *82* (12), 125416.
(3) Buiel, E.; Dahn, J. R. *Electrochim. Acta* **1999**, *45* (1), 121−130.
(4) Zheng, H.; Qu, Q.; Zhang, L.; Liu, G.; Battaglia, V. S. *RSC Adv.* **2012**, *2* (11), 4904.
(5) Chan, K. K.; Amaratunga, G. a J.; Shafi, Z. a; Ashburn, P.; Wong, S. P. *Diamond Relat. Mater.* **1993**, *2*, 1445−1448.
(6) Ilie, A.; Conway, N.; Kleinsorge, B.; Robertson, J.; Milne, W. *J. Appl. Phys.* **1998**, *84* (1998), 5575−5582.
(7) Ma, Z. Q.; Liu, B. X. *Sol. Energy Mater. Sol. Cells* **2001**, *69* (4), 339−344.
(8) Fadzilah, A. N.; Dayana, K.; Rusop, M. *Int. J. Photoenergy* **2013**, *2013*, 1−7.
(9) Bernardi, M.; Lohrman, J.; Kumar, P. V.; Kirkeminde, A.; Ferralis, N.; Grossman, J. C.; Ren, S. *ACS Nano* **2012**, *6* (10), 8896−8903.
(10) Wang, X.; Zhi, L.; Müllen, K. *Nano Lett.* **2008**, *8* (1), 323−327.
(11) Yin, Z.; Sun, S.; Salim, T.; Wu, S.; Huang, X.; He, Q.; Lam, Y. M.; Zhang, H. *ACS Nano* **2010**, *4* (9), 5263−5268.
(12) Becerril, H. A.; Mao, J.; Liu, Z.; Stoltenberg, R. M.; Bao, Z.; Chen, Y. *ACS Nano* **2008**, *2* (3), 463−470.
(13) Eda, G.; Fanchini, G.; Chhowalla, M. *Nat. Nanotechnol.* **2008**, *3* (5), 270−274.
(14) Reina, A.; Jia, X.; Ho, J.; Nezich, D.; Son, H.; Bulovic, V.; Dresselhaus, M. S.; Kong, J. *Nano Lett.* **2009**, *9* (1), 30−35.
(15) Li, X.; Cai, W.; An, J.; Kim, S.; Nah, J.; Yang, D.; Piner, R.; Velamakanni, A.; Jung, I.; Tutuc, E.; Banerjee, S. K.; Colombo, L.;

DOI: 10.1021/acs.nanolett.5b04735
Nano Lett. XXXX, XXX, XXX−XXX

Ruoff, R. S. *Science (Washington, DC, U. S.)* **2009**, *324* (5932), 1312−1314.
(16) Li, X.; Zhu, Y.; Cai, W.; Borysiak, M.; Han, B.; Chen, D.; Piner, R. D.; Colombo, L.; Ruoff, R. S. *Nano Lett.* **2009**, *9* (12), 4359−4363.
(17) Maize, K.; Das, S. R.; Sadeque, S.; Mohammed, A. M. S.; Shakouri, A.; Janes, D. B.; Alam, M. A. *Appl. Phys. Lett.* **2015**, *106*, 143104.
(18) Raji, A. O.; Varadhachary, T.; Nan, K.; Wang, T.; Lin, J.; Genorio, B.; Zhu, Y.; Kittrell, C.; Tour, J. M. *ACS Appl. Mater. Interfaces* **2016**, *8*, 3551.
(19) Sui, D.; Huang, Y.; Huang, L.; Liang, J.; Ma, Y.; Chen, Y. *Small* **2011**, *7* (22), 3186−3192.
(20) Tunability is defined here as the ability to change a specific property of a material to a desired value and not the reversibility of the property after processing to a different desired value.
(21) Kuhner, G.; Manfred, V. In *Carbon Black Science and Technology*; Donnet, J.-B., Bansal, R. C., Meng-Jiao, W., Eds.; CRC Press: Boca Raton, FL, 1993; pp 1−66.
(22) Robertson, J. *Adv. Phys.* **1986**, *35*, 317−374.
(23) Weiler, M.; Sattel, S.; Giessen, T.; Jung, K.; Ehrhardt, H.; Veerasamy, V.; Robertson, J. *Phys. Rev. B: Condens. Matter Mater. Phys.* **1996**, *53* (3), 1594−1608.
(24) Lee, J.-H.; Lee, E. K.; Joo, W.; Jang, Y.; Kim, B.; Lim, J. Y.; Choi, S.-H.; Ahn, S. J.; Ahn, J. R.; Park, M.; Yang, C.; Choi, B. L.; Hwang, S.; Whang, D. *Science* **2014**, *344* (6181), 286−289.
(25) Zhou, H.; Yu, W. J.; Liu, L.; Cheng, R.; Chen, Y.; Huang, X.; Liu, Y.; Wang, Y.; Huang, Y.; Duan, X. *Nat. Commun.* **2013**, *4*, 2096.
(26) U.S. Energy Information Administration. *Annual Energy Review*. http://www.eia.gov/coal/data.cfm (accessed August 2015).
(27) Levine, D. G.; Schlosberg, R. H.; Silbernagel, B. G. *Proc. Natl. Acad. Sci. U. S. A.* **1982**, *79* (10), 3365−3370.
(28) Dindi, H.; Bai, X.; Krantz, W. B. *Fuel* **1989**, *68* (2), 185−192.
(29) Duba, A. G. *Fuel* **1977**, *56* (4), 441−443.
(30) *The Penn State Coal Sample Bank And Database*; 1998. http://www.energy.psu.edu/copl/doesb.html (accessed August 2015).
(31) Cumming, J. W.; McLaughlin, J. *Thermochim. Acta* **1982**, *57* (3), 253−272.
(32) Ferrari, A. C.; Robertson, J. *Phys. Rev. B: Condens. Matter Mater. Phys.* **2000**, *61* (20), 14095−14107.
(33) Ferrari, A.; Robertson, J. *Phys. Rev. B: Condens. Matter Mater. Phys.* **2001**, *64* (7), 075414.
(34) Tuinstra, F.; Koenig, L. *J. Chem. Phys.* **1970**, *53* (3), 1126−1130.
(35) Lucchese, M. M.; Stavale, F.; Ferreira, E. H. M.; Vilani, C.; Moutinho, M. V. O.; Capaz, R. B.; Achete, C. a.; Jorio, a. *Carbon* **2010**, *48* (5), 1592−1597.
(36) Ferrari, A. C.; Basko, D. M. *Nat. Nanotechnol.* **2013**, *8* (4), 235−246.
(37) Kuzmany, H.; Pfeiffer, R.; Salk, N.; Günther, B. *Carbon* **2004**, *42* (5−6), 911−917.
(38) Tauc, J.; Grigorovici, R.; Vancu, A. *Phys. Status Solidi B* **1966**, *15* (2), 627−637.
(39) Davis, E. a.; Mott, N. F. *Philos. Mag.* **1970**, *22* (179), 0903−0922.
(40) Robertson, J. *Prog. Solid State Chem.* **1991**, *21* (4), 199−333.
(41) Robertson, J.; O'Reilly, E. *Phys. Rev. B: Condens. Matter Mater. Phys.* **1987**, *35* (6), 2946−2957.
(42) Apsley, N.; Hughes, H. P. *Philos. Mag.* **1975**, *31* (6), 1327−1339.
(43) Eda, G.; Mattevi, C.; Yamaguchi, H.; Kim, H.; Chhowalla, M. *J. Phys. Chem. C* **2009**, *113* (35), 15768−15771.
(44) Kaiser, A. B.; Gómez-Navarro, C.; Sundaram, R. S.; Burghard, M.; Kern, K. *Nano Lett.* **2009**, *9* (5), 1787−1792.
(45) Hauser, J. J. *Solid State Commun.* **1975**, *17*, 1577−1580.
(46) Shimakawa, K.; Miyake, K. *Phys. Rev. B: Condens. Matter Mater. Phys.* **1989**, *39* (11), 7578−7584.
(47) Hussain, A. M.; Lizardo, E. B.; Torres Sevilla, G. A.; Nassar, J. M.; Hussain, M. M. *Adv. Healthcare Mater.* **2015**, *4* (5), 665−673.
(48) Kim, D. H.; Wang, S.; Keum, H.; Ghaffari, R.; Kim, Y. S.; Tao, H.; Panilaitis, B.; Li, M.; Kang, Z.; Omenetto, F.; Huang, Y.; Rogers, J. A. *Small* **2012**, *8* (21), 3263−3268.
(49) Song, S. H.; Kwak, B. S.; Park, J. S.; Kim, W.; Jung, H. IL. *Sens. Actuators, A* **2009**, *151* (1), 64−70.
(50) Coskun, S.; Selen Ates, E.; Emrah Unalan, H. *Nanotechnology* **2013**, *24* (12), 125202.
(51) Wang, P.-H.; Chen, S.-P.; Su, C.-H.; Liao, Y.-C. *RSC Adv.* **2015**, *5*, 98412−98418.
(52) Kozłowska, A.; Gawlik, G.; Szewczyk, R.; Piątkowska, A.; Krajewska, A. *OSA Technol. Dig.* **2014**.
(53) Sánchez-González, J.; Macías-García, A.; Alexandre-Franco, M. F.; Gómez-Serrano, V. *Carbon* **2005**, *43* (4), 741−747.
(54) Probst, N. In *Carbon Black Science and Technology*; Donnet, J., Bansal, R. C., Wang, M.-J., Eds.; CRC Press: Boca Raton, FL, 1993; pp 271−288.
(55) Cho, N.-H.; Krishnan, K. M.; Veirs, D. K.; Rubin, M. D.; Hopper, C. B.; Bhushan, B.; Bogy, D. B. *J. Mater. Res.* **1990**, *5* (11), 2543−2554.
(56) Jones, D. I.; Stewart, a. D. *Philos. Mag. B* **1982**, *46* (5), 423−434.
(57) Park, Y. S.; Cho, H. J.; Hong, B. *J. Korean Phys. Soc.* **2007**, *51* (3), 1119.
(58) Savvides, N. *J. Appl. Phys.* **1986**, *59* (12), 4133−4145.

DOI: 10.1021/acs.nanolett.5b04735
Nano Lett. XXXX, XXX, XXX−XXX